Graphical Abstract

Hexafluoroacetylacetonate (hfac) as ligand for pentamethylcyclopentadienyl (Cp*) rhodium and iridium complexes: Some surprising results, including an $Ir_3Na_1O_4$ cubane structure.

Christine M. DuChane,Joseph S. Merola

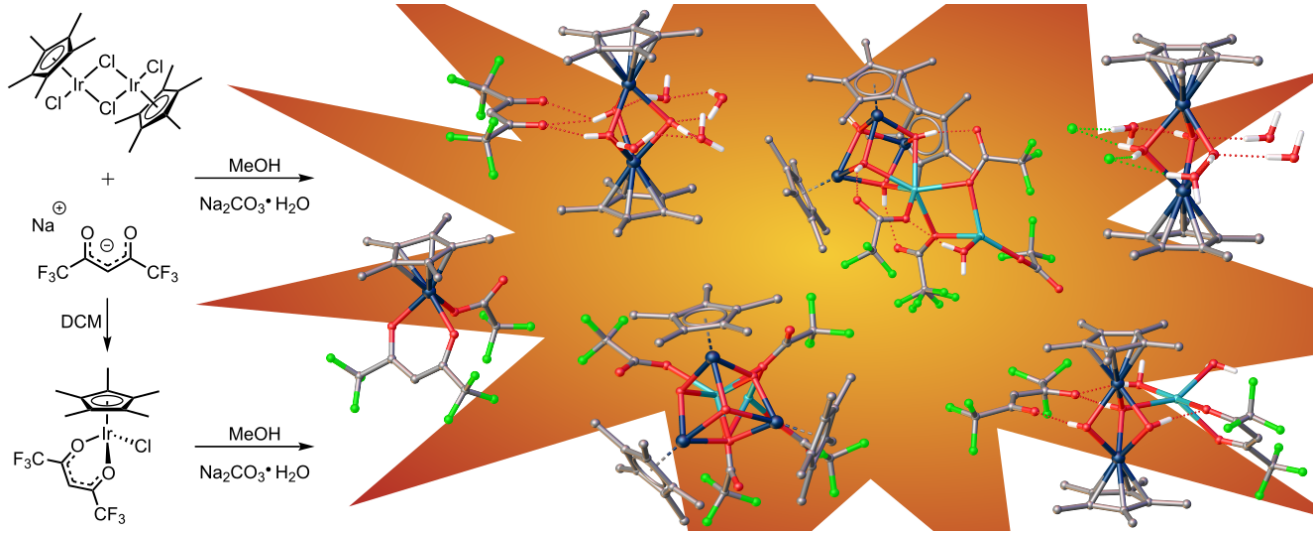

The reaction of $[Cp^*IrCl_2]_2$ and hfacNa proceeded as expected in DCM to yield Cp*Ir(1,1,1,5,5,5-hexafluoroacetylacetonate)Cl, but the analogous reaction or further reaction in the presence of MeOH and sodium carbonate gave a surprising array of unexpected products.

Highlights

Hexafluoroacetylacetonate (hfac) as ligand for pentamethylcyclopentadienyl (Cp*) rhodium and iridium complexes: Some surprising results, including an $Ir_3Na_1O_4$ cubane structure.

Christine M. DuChane,Joseph S. Merola

- Reaction of $[Cp^*MCl_2]_2$ (M = Rh, Ir) with 1,1,1-trifluoroacetylacetone (tfac) proceeded as expected to give Cp*M(tfac)Cl, as did reaction of $[Cp^*MCl_2]_2$ (M = Rh, Ir) with sodium hexafluoroacetylacetonate (hfacNa) in dichloromethane to give Cp*M(hfac)Cl
- Reaction of Cp*Ir(hfac)Cl with $Na_2CO_3 \cdot H_2O$ in methanol led to a variety of decomposition products, including two $Ir_3Na_1O_4$ cubane structures

Hexafluoroacetylacetonate (hfac) as ligand for pentamethylcyclopentadienyl (Cp*) rhodium and iridium complexes: Some surprising results, including an $Ir_3Na_1O_4$ cubane structure.

Christine M. DuChane, Joseph S. Merola*

Department of Chemistry, Virginia Tech, Blacksburg, VA 24061, USA

ARTICLE INFO

Keywords:
iridium
hexafluoroacetylacetonato
iridium cluster
crystals
piano stool

ABSTRACT

Attempts to prepare hexafluoroacetylacetonate (hfac) piano stool complexes of pentamethylcyclopentadienyl Cp* iridium and rhodium led to a surprising array of unexpected products. The desired complex, Cp*M(hfac)Cl, was obtained following the reaction of sodium hexafluoroacetylacetonate (hfacNa) with $[Cp^*MCl_2]_2$ in dichloromethane. Variations of this synthetic method resulted in twelve unique crystallographically identified products, eleven of which contain the hfac ligand or a trifluoroacetylacetonate (TFA) ligand, either coordinated to the metal or as a non-coordinating anion. Five dinuclear Cp* iridium hydroxo-bridged products with various fluorinated non-coordinating anions were obtained. The most intriguing two complexes are trinuclear Cp^*Ir^{III} hydroxo-bridged clusters that have, at their core, an Ir_3NaO_4 cubane structure. Attempts to devise rational syntheses of the hydroxo-bridged cluster compounds were not successful. Generation of the TFA moieties likely occurred following degradation of Cp*M(hfac)Cl. The reaction between $[Cp^*MCl_2]_2$ and 1,1,1-trifluoroacetylacetonate (tfac) proceeded as expected to give Cp*M(tfac)Cl with no observed side product formation, indicating that the metal-coordinated tfac moiety is significantly more stable than the metal-coordinated hfac moiety.

1. Introduction

Hexafluoroacetylacetonate (hfac) is an extremely well known β-diketonato ligand that has been used extensively in precursor complexes for chemical vapor deposition (CVD) of metals due to the relatively high volatility of these complexes [1–4].

Numerous noble metal hfac complexes have been synthesized, including several varieties of iridium and rhodium complexes. The tris β-diketonato complexes $M(hfac)_3$ (M = Ir, Rh) may be prepared from the reaction of hfac with $M(OH)_3$ [5, 6]. $Ir(hfac)_3$ is also prepared through the reaction of $IrCl_3 \cdot xH_2O$ and hfac under inert conditions, [7] though the analogous reaction with rhodium has been found to yield $RhCl(hfac)_2 \cdot 3\,H_2O$ rather than the tris β-diketonato complex. Upon sublimation, the chloro-bridged dimer $[(hfac)_2RhCl]_2$ is formed [8]. The acetate-bridged dimer rhodium(II) $[(hfac)Rh(H_2O)(OAc)]_2$ is synthesized by reacting hfacH with $[Rh(OAc)_2(H_2O)]_2$ in water [9]. The synthesis and characterization of (cod)Rh(hfac) was reported in 1988 from the reaction of $[(cod)RhCl]_2$ with hfacH under basic conditions [10].

Metal complexes of hfac have shown susceptibility to further reaction in basic aqueous solution. Complexes of cobalt and chromium featuring $[hfac]^-$ were found to react with anionic species including hydroxide or methoxide to produce the dianionic species $[hfacX]^{2-}$ that can also act as a chelating ligand (Figure 1) [11–13].

Recently, we reported on the synthesis, structure and biological activity of pentamethyl and tetramethyl-R cyclopentadienyl iridium(III) and rhodium(III) piano stool complexes featuring a range of β-diketonato ligands [14]. It seemed to be a natural fit that hexafluoroacetylacetonato complexes of iridium and rhodium should be a part of this investigation. However, we discovered that this chemistry did not proceed as expected and instead produces some very intriguing structures resulting from the decomposition of hexafluoroacetylacetonate iridium species. In this paper, we present these results and single crystal X-ray diffraction studies of some very unusual iridium compounds.

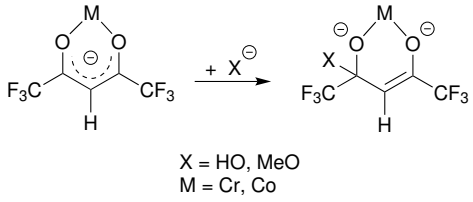

Figure 1: Reaction of metal-coordinated hfac with hydroxide or methoxide to give a dianionic species [13].

2. Synthesis

The synthesis of Cp*M(tfac)Cl (**1-Ir** and **1-Rh**) proceeded rapidly and with no side products from the reaction of $[Cp^*MCl_2]_2$ with 1,1,1-trifluoroacetylacetone (tfac) and $Na_2CO_3 \cdot H_2O$ in either DCM or methanol. Cp*Ir(hfac)Cl (**2-Ir**) was obtained in good yield and purity via the reaction of $[Cp^*IrCl_2]_2$ and 4 equivalents of sodium hexafluoroacetylacetonate (hfacNa) in DCM for approximately one hour. For rhodium, this method yielded Cp*Rh(hfac)Cl

*Corresponding author
jmerola@vt.edu (J.S. Merola)
ORCID(s): 0000-0001-9575-3424 (C.M. DuChane); 0000-0002-1743-1777 (J.S. Merola)

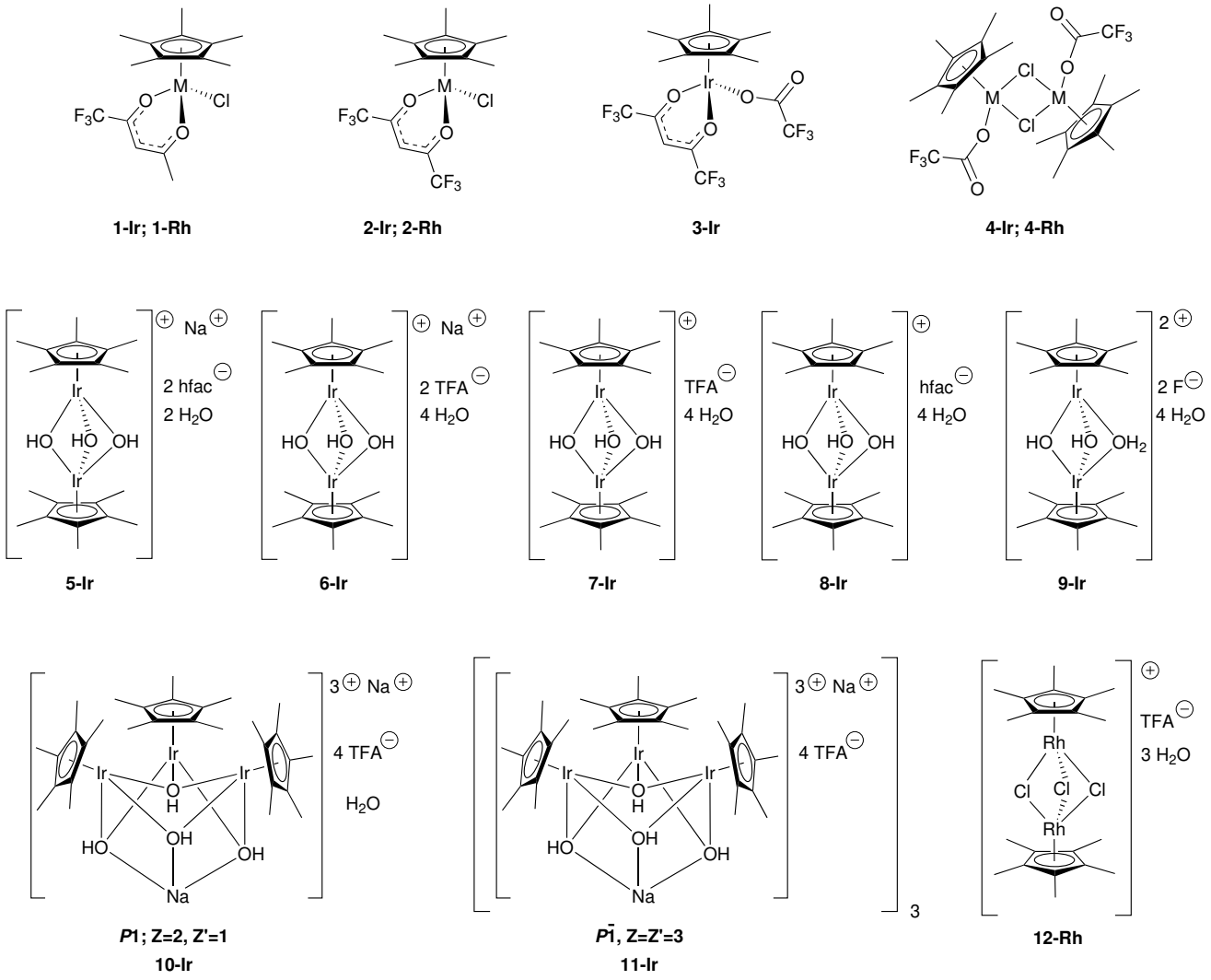

Figure 2: Structures of the products discussed in this article. All complexes were identified crystallographically. Only the core structures of complexes 5–12, which are likely degradation products from complexes 1–4, are shown here in order to simplify the comparison. The full structures are shown in Section 6.3.

(**2-Rh**) in addition to small quantities of the chloro-bridged rhodium dimers $[Cp^*Rh(\mu\text{-}Cl)(TFA)]_2$ (**4-Rh**) and $[(Cp^*Rh)_2(\mu\text{-}Cl)_3]^+[TFA]^-$ (**12-Rh**). Cp*Ir(hfac)(TFA) (**3-Ir**) was synthesized quantitatively from the reaction of **2-Ir** with AgTFA in $CDCl_3$. $[Cp^*M(\mu^2\text{-}Cl)(TFA)]_2$ (**4-Ir** and **4-Rh**) was obtained in good yield and purity from the reaction of $[Cp^*MCl_2]_2$ with AgTFA in dry benzene.

For syntheses involving TFA or hfac, dissolution in methanol and addition of $Na_2CO_3 \cdot H_2O$ to either the reaction mixtures or the isolated products was found to give a number of unique products in addition to the desired complexes (Figure 2). Of these unique products, a number of complexes were identified crystallographically.

3. Structural commentary

Tables with selected relevant bond lengths are given in the ESI (iridium complexes: Table S1; rhodium complexes: Table S2).

3.1. Iridium complexes

3.1.1. Iridium complexes with η^2-diketonato ligands

Three iridium complexes (**1-Ir**, **2-Ir**, and **3-Ir**; Figures 4, 5, and 6, respectively) contain the fluorinated β-diketonato ligand chelating through both oxygen atoms in a bidentate binding mode typical of acetylacetonate (acac) complexes. A search of the 2019 Cambridge Structural Database (CSD) [15] for iridium acetylacetonate-type complexes found 463 iridium moieties with an η^2– coordinated β-diketone ligand, showing a minimum Ir–O bond length of 1.991 Å to a maximum of 2.224 Å, with a mean of 2.115 Å. Two complexes were found in the CSD containing the intact tfac ligand coordinated to iridium, while six complexes were found containing the intact hfac ligand coordinated to iridium. The average Ir–O length for **1-Ir**, **2-Ir**, and **3-Ir** is 2.11(1) Å, which falls near the average of the reported range for Ir–β-diketone ligands.

3.1.2. Iridium complexes with η^1-TFA ligands

Two structures (**3-Ir** and **4-Ir**, Figures 6 and 7, respectively) contain iridium-bound η^1-trifluoroacetate ligands. A CSD search of the [Ir–TFA] moiety found 39 examples with a mean Ir–O distance of 2.119(3) Å and an Ir–O–C bond angle ranging from a minimum of 115.73° to a maximum of 137.22° with a mean of 125.6°. For **3-Ir** and **4-Ir**, the Ir–O distances for the oxygen atom in the TFA ligand were 2.118(5) Å and 2.112(4) Å, and the Ir–O–C bond angles are 125.7(4)° and 120.4(4)°, respectively, indicating that the η^1-TFA ligands for the complexes reported here are relatively "normal" compared with those in the literature.

3.1.3. Dinuclear hydroxo-bridged iridium complexes

5-Ir, **6-Ir**, **7-Ir**, and **8-Ir** (Figures 8–11, respectively) are dinuclear iridium(III) complexes with three bridging hydroxo groups in a hydrogen-bonding interaction with water molecules and fluorinated non-coordinating ligands. This $[Cp^*Ir(\mu^2\text{-}OH)_3IrCp^*]^+$ core has appeared previously in the literature with different counterions and varying numbers of waters of hydration H–bonded to the bridging OH ligands [16–19].

5-Ir and **6-Ir** each contain the $[Cp^*Ir(\mu^2\text{-}OH)_3IrCp^*]^+$ core with two structurally identical non-coordinating anions (hfac and TFA, respectively) and a sodium cation. In both cases, one molecule of the non-coordinating fluorinated ligand is in a hydrogen-bonding interaction with two of the bridging OH protons, while the other fluorinated ligand and two water molecules are bonded to Na1. **5-Ir** crystallized in the space group $P\bar{1}$ (#2) while **6-Ir** crystallized in the space group $P2_1/n$ (#14). The TFA–Na1 moiety in **6-Ir** is situated about an inversion center such that two moieties form an 8-membered ring. **5-Ir** contains two molecules of water while **6-Ir** contains four molecules of water in the asymmetric unit.

7-Ir contains a single non-coordinating TFA anion and **8-Ir** contains a single non-coordinating hfac anion. Both structures crystallized in the space group $P\bar{1}$ and contain four molecules of water hydrogen-bonded to the bridging OH ligands. In both cases, the oxygen atoms of the fluorinated ligand are also hydrogen-bonded to the bridging hydroxo ligands.

9-Ir (Figure 12) is a dinuclear iridium(III) complex that appears to contain two non-coordinating fluoride anions. **9-Ir** crystallized in the space group $P2_1/m$ with Ir1, Ir2, O3, C1, C4, C7, and C10 in special positions on the mirror plane. Unlike **5-Ir** and **6-Ir**, we did not locate a non-coordinating cation, leading to somewhat of a charge discrepancy. This charge discrepancy may be justified by either considering disorder to the non-coordinating atoms, or alternatives to the tris-hydroxo bridging atoms. Our best intuition suggests this structure likely contains two bridging hydroxo groups and one bridging water. As O3 is the only bridging group that lies on the mirror plane, it is tempting and logical to place the bridging water moiety at this position.

3.1.4. Trinuclear hydroxo-bridged iridium complexes

10-Ir is a trinuclear Ir cluster bridged by four hydroxo groups with two Na atoms, four distinct TFA units, one water molecule, and one acetone molecule (Figure 13). The vertices of the cube include three Ir atoms, four O atoms and one Na atom. One TFA group (O5/O6) is singly bonded to Na1 but also has strong hydrogen-bonding to a hydrogen atom of one of the OH vertices of the cube (O9···H – O2) as well as to an H atom on the water molecule bonded to Na2. Two TFA units (O7/O8 and O11/O12) bridge the cube Na atom (Na1) and the non-cube Na atom (Na2). Additionally, both of those bridging TFA units have strong hydrogen-bonding between the "carbonyl" oxygen and the hydrogen of one of the OH vertices of the cube (O8···H – O4 and O12···H – O3). The fourth TFA unit (O9/O10) is coordinated η^1 to the Na atom that is not part of the cube (Na2) and has a hydrogen-bonding interaction with a hydrogen of one of the OH vertices (O1) of a neighboring crystallographically equivalent cubane molecule.

Single crystals containing the cluster unit were grown and solved in two different unit cells. Both structures were solved in triclinic space groups, with one of the structures (**10-Ir**) in $P\bar{1}$ (#2) with Z=2 (Z'=1) and the other (**11-Ir**) in $P1$ (#1) with Z=Z'=3. The solved structures show the same core, with the exception that **11-Ir** does not contain a water molecule coordinated to Na2 (Figure 14). Otherwise, the core atom arrangement is identical between all four unique molecules, though slight rotational and positional differences occur between the Cp* moieties and the TFA units. **11-Ir** was numbered analogously to **10-Ir** for convenience.

While cubane structures are not uncommon in the literature – over 2000 entries in the Cambridge Structural Database [20, 21] – structurally characterized iridium-containing cubes are quite rare. Only a few Ir_4S_4 cubes are known [22], and though there are no isolated iridium containing cubanes with oxygen, an iridium-μ-oxo tetranuclear cubane species has recently been proposed as a resting state in molecular iridium-based water oxidation [23]. Based on these literature results, a cluster with three Ir atoms, four O atoms and one Na atom at the vertices is an extremely unlikely combination.

The average Ir–Ir distance is 3.071(5) Å for all 10 metal centers in the 5 dinuclear hydroxo-bridged complexes and 3.42(1) Å for the 12 metal centers in **10-Ir**, so there is no evidence for Ir–Ir bonding in any of these complexes. The average Ir–O bond length for all 60 Ir–μ^2-O bonds within the hydroxo-bridged complexes reported here is 2.12(4) Å (range: 2.074–2.213 Å), with both the 10 longest and 10 shortest lengths occurring in the trinuclear complexes. The literature average (5 structures, 30 Ir–μ^2-O bonds) is 2.12(1) Å (range: 2.098–2.153 Å). While the average Ir–O bond length of the complexes reported here aligns with the literature average, the cluster moieties do contain a number of significantly longer and shorter Ir–O bonds than appears to be typical for multinuclear hydroxo-bridged Cp*Ir complexes. In all cases, the positions of the hydrogen atoms on the bridging hydroxo and non-coordinating water molecules were somewhat difficult to locate definitively. Tables with selected relevant bond lengths

are given in the ESI (iridium complexes: Table S1)

3.2. Rhodium complexes

3.2.1. Rhodium complexes with η^2-diketonato ligands

Two rhodium structures (**1-Rh** and **2-Rh**, Figures 15 and 16, respectively) were found to contain a fluorinated ligand chelating through both oxygen atoms in a bidentate binding mode. The average Rh–O bond length was found to be 2.11(1) Å, which is on the slightly high end of the CSD average of 2.069(45) (296 instances of η^2– rhodium-coordinated β-diketonato ligands) but still well within the range of 1.964–2.275 Å.

3.2.2. Dinuclear rhodium complexes

4-Rh (Figure 18) is a dirhodium complex with two bridging chlorides and a TFA group bound to each rhodium in an η^1– manner. The Rh–O bond length and Rh–O–C bond angle for **4-Rh** is 2.121(2) Å and 120.6(2)°, respectively. Only 42 of the 248 Rh–TFA instances in the CSD contained Rh–η^1-TFA moieties. Of these, the mean Rh–O bond length was 2.09(8) Å with the Rh–O–C angle ranging from 97.67–134.39° (mean of 124.8°).

12-Rh (Figure 17) is also a dirhodium complex, but features three bridging chlorides and a non-coordinated TFA anion. Sixteen tri-μ-chloro-bis[Cp*Rh(III)] complexes containing a variety of non-coordinating anions appear in the CSD with an average Rh–Rh distance of 3.211 Å and an average Rh–Cl bond length of 2.4565 Å [24–34]. **12-Rh** has a Rh–Rh distance of 3.2159(4) Å, indicating there is no Rh–Rh bond, and an average Rh–Cl bond length of 2.4577 Å. Though this structure seems "normal" with regards to bond lengths, there is an interesting hydrogen bonding network of water and TFA molecules that does not occur in the other structures discussed in this paper, nor did we find it in the CSD. Two molecules of non-coordinating anionic TFA form a 16 atom H-bonded ring with 4 water molecules oriented about an inversion center. The 16-atom rings are connected via three interconnected 4-membered rings, also oriented along an inversion center (Figure 3). These layers alternate with layers of the rhodium complex, with a weak hydrogen bond between a fluorine atom on one of the TFA moieties and a methyl group of a neighboring Cp* moiety.

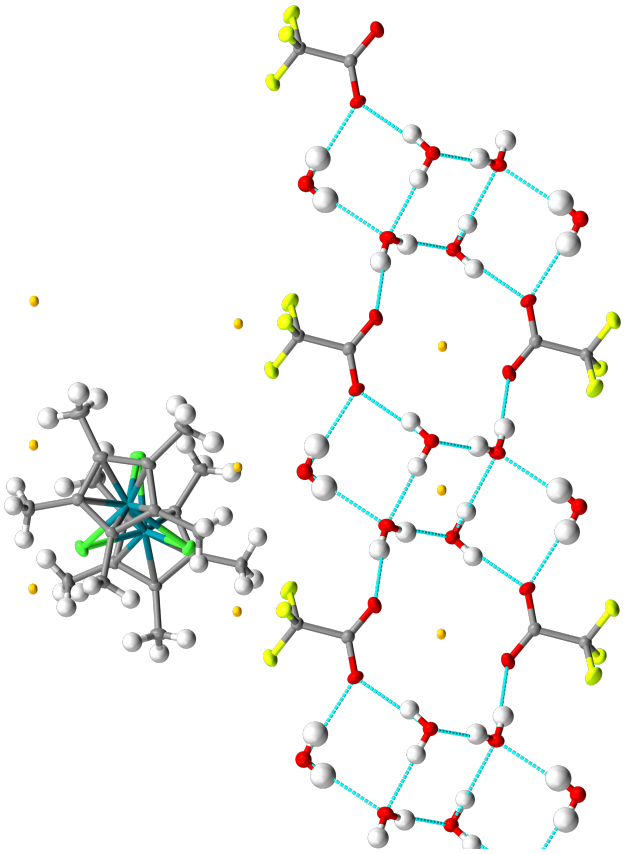

Figure 3: 12-Rh viewed down the C-axis. Inversion centers are shown as orange dots.

4. Discussion

4.1. Investigation into unexpected complexes

The large variety and number of unexpected complexes may have originated from decay of the hfac or TFA metal-coordinated moieties in the presence of $Na_2CO_3 \cdot H_2O$ and MeOH. To probe this theory, one equivalent of $Na_2CO_3 \cdot H_2O$ per iridium center was added to solutions of **2-Ir**, **3-Ir**, and **4-Ir** in MeOH and stirred for 30 minutes at room temperature. The MeOH was then removed under reduced pressure and NMR samples of the yellow residues were made in $CDCl_3$. Crystals of the products of each reaction were grown via slow diffusion of hexanes into a saturated acetone solution. Analysis of these crystals revealed that **5-Ir** is formed via degradation of **2-Ir**, both **5-Ir** and **6-Ir** are formed via degradation of **3-Ir**, and **7-Ir** is formed via degradation of **4-Ir** (Table 1).

Table 1
Degradation products obtained from reaction with $Na_2CO_3 \cdot H_2O$ in MeOH.

Starting complex	Product obtained
2-Ir	**5-Ir**
3-Ir	**5-Ir**, **6-Ir**
4-Ir	**7-Ir**

In several cases, reactions between $[Cp^*MCl_2]_2$ and hfacNa produced products containing trifluoroacetate moieties, which likely originated from the decomposition of hfac in the presence of water under basic conditions [35]. Consequently, it seemed reasonable that the TFA containing products observed here could be synthesized rationally using trifluoroacetate salts with $[Cp^*IrCl_2]_2$ in the same solvent systems as the reactions of the hfac salts. Several attempts were made to synthesize **10-Ir** or **11-Ir** intentionally via reaction between the Cp* iridium(III) chloride dimer and AgTFA or NaTFA in acetone and methanol; however, we were unable to directly synthesize either cluster. Despite this, **10-Ir** and **11-Ir** grew from solutions of **5-Ir**, indicating that the clusters are likely produced via decay of **5-Ir**.

4.2. Additional characterization

Due to complexities determining the identities of the complexes via standard characterization techniques, identification was primarily driven via analysis of the single crystal X-ray structures.

4.2.1. NMR

Synthesis of **1-Ir**, **1-Rh**, **2-Ir**, **3-Ir**, **4-Ir**, and **4-Rh** consistently proceeded to give pure products that were easily characterizable via NMR. NMR analysis of the hydroxo-bridged products (**5-Ir**–**11-Ir**) was surprisingly complicated due to the relatively small number of moieties in each complex that give easily observable, uniquely discernible ^{1}H-NMR signals. All products gave signals attributable to the Cp* moiety, though many such signals overlapped, and products with intact hfac ligands gave signals attributable to the C3-proton on the ligand. Bridging hydroxo and coordinated water molecules also showed unique signals, though these signals were less discernible due to H/D exchange as well as the tendency of these signals to shift based on temperature and the presence of other components or solvent in the sample. Following crystallographic identification of these complexes, NMR samples were made of the pure crystals when possible; from this, the components in $CDCl_3$ solution were identified.

Many of the compounds were somewhat insoluble in $CDCl_3$; consequently, several expected ^{13}C NMR signals were too weak for clear observation within a reasonable experimental time frame. The only consistently present ^{13}C NMR signals were attributable to the Cp*CH_3 and Cp*C carbon atoms. The carbon signals of the hfac and TFA ligands were often missing from the spectra, likely because they are multiplets due to C–F coupling, which weakens the signal.

Deuterated acetone was explored as an NMR solvent in several cases; however, many of the samples appear to degrade in solution, as evidenced by the appearance of new signals and disappearance of old signals concurrent with a change in the sample color from yellow or orange to brown. Solutions containing complexes with non-coordinating anions were also found to decay in $CDCl_3$ solution or when evaporated from $CDCl_3$ solution under vacuum.

4.2.2. High-Resolution Mass Spectrometry (HRMS)

In an attempt to further characterize the products of these reactions, HRMS isotope patterns were assessed, both for bulk powders containing multiple products as well as for the isolated pure products. It is noteworthy that the only isolated products that gave the expected monoisotopic mass and pattern were **1-Ir**, **1-Rh**, and **2-Rh**. Many complexes gave a similar isotopic pattern with a monoisotopic mass around 703.169; however, we were unable to identify this fragment. Each mixture also contained many other fragments that were unidentifiable.

A common ion with an averaged monoisotopic mass of 763.1591 was found in several cases. This signal was found to match the isotopic pattern and mass of $[C_{22}H_{33}Ir_2O_5]^+$, which likely corresponds to either the ion $[\{Cp^*Ir\}_2\{HCO_2\}_2\{OH\}]^+$ or the ion $[\{Cp^*Ir\}_2\{HCO_2\}\{CO_2\}\{OH_2\}]^+$. Several signals were also found for these products that correspond with the sequential loss of [CO] and [H_2O] fragments from this ion. The source of the [CO_2] containing fragments may have been the formic acid in the mobile phase of the LC-HRMS system used; however, metal TFA and hfac containing complexes have also been known to ionize with loss of a [CF_3] fragment [36, 37]. Ultimately, the HRMS traces of these products corroborate the highly reactive nature of these metal complexes.

4.2.3. Powder X-ray diffraction

The majority of the bulk samples had poor crystallinity and gave very weak powder patterns. Additionally, many of the samples that were not too amorphous for analysis did not match the calculated patterns, suggesting that the single crystals isolated and solved are not necessarily representative of the bulk material. For the hydroxo-bridged complexes, the lack of match could simply be due to a lack of solvent molecules in the bulk powders; however, it is also likely that many samples contained multiple products. Interestingly, the bulk samples from which **10-Ir** and **11-Ir** grew were found to match the calculated PXRD pattern of **5-Ir**, rather than the expected powder pattern calculated from the trinuclear crystals (Figure S1). This corroborates the posit that the cluster crystals likely grew from degradation of **5-Ir** in solution.

5. Conclusions

Though metal complexes of hfac are extremely common in the literature, the preparation of Cp*Ir(hfac)Cl from $[Cp^*IrCl_2]_2$ and hfac led to the expected product in DCM but was relatively unsuccessful in other solvent systems. Instead, reactions in the presence of MeOH and $Na_2CO_3 \cdot H_2O$ led to a variety of products, eleven of which were characterized by single crystal X-ray crystallography, including two $[Cp^*Ir]_3$ clusters and five $[Cp^*Ir]_2$ dimers, all bridged by hydroxo groups. The most unique and intriguing structures found in this study are the cluster compounds, **10-Ir** and **11-Ir**. While we have yet to find the correct conditions to make these clusters rationally, future work will continue since such a cluster is likely to have very interesting redox chemistry [38, 39].

While not known with certainty, it would appear that the well-characterized complexes 1–4 undergo decomposition in the presence of $Na_2CO_3 \cdot H_2O$ and MeOH, leading to the formation of the observed decomposition products. The exact mechanism of the formation of these products is more complicated than simply reaction with hfac constituents, however, since attempts to make the cluster intentionally were not successful. There were no issues with using 1,1,1-trifluoroacetylacetonate (tfac) as a ligand and the expected Cp*M(tfac)Cl complexes (M = Rh, Ir) were formed in good yield and purity.

6. Experimental

6.1. Materials

Rhodium and iridium dimers $[Cp^*MCl_2]_2$ were synthesized as reported previously [40]. Reagent grade solvents and all other materials for synthesis, purification, and characterization were purchased from commercial sources and used as received unless otherwise stated. Sodium hexafluoroacetylacetonate, thallium hexafluoroacetylacetonate, sodium trifluoroacetate, and silver trifluoroacetate were purchased from Strem Chemicals (Newburyport, MA 01950). Deuterated solvents for NMR spectroscopy were obtained from Cambridge Isotope Laboratories.

6.2. Instrumentation

^{1}H NMR, ^{13}C NMR, and ^{19}F NMR spectra were collected on a Varian MR-400 NMR spectrometer. ^{13}C and ^{19}F NMR were correspondingly recorded at 101 and 376 MHz, respectively. HRMS were collected on an Agilent 6220 Accurate Mass TOF LC-MS. X-ray crystallographic data for **3-Ir**, **4-Ir**, **7-Ir**, and **10-Ir** were collected at 100K on a Rigaku Oxford Diffraction Gemini E Ultra operating with Mo Kα radiation. X-ray crystallographic data for **1-Ir**, **1-Rh**, **2-Ir**, **2-Rh**, **4-Rh**, **5-Ir**, **6-Ir**, **8-Ir**, **9-Ir**, **11-Ir**, and **12-Rh** were collected at 100K on a Rigaku Oxford Diffraction Synergy operating with Mo Kα radiation. Data collection and data reduction were performed using Agilent's CrysAlisPro software [41]. Structure solution was performed using SHELXT-201430 [42] and refined using SHELXL-201431 via Olex2. The final refinement model involved anisotropic displacement parameters for non-hydrogen atoms and a riding model for all hydrogen atoms. Olex2 was used for molecular graphics generation [43]. Searches of the Cambridge Structural Database [15] were carried out using the program Conquest [44] and the results were analyzed with the statistical functions of the program Mercury [20, 21].

6.3. Synthesis and Characterization

6.3.1. Iridium complexes

*Synthesis of **1-Ir**.* A round-bottom flask was charged with $[Cp^*IrCl_2]_2$ (0.0581 g, 0.0729 mmol), trifluoroacetylacetone (0.0195 mL, 0.1604 mmol), and $Na_2CO_3 \cdot H_2O$ (0.0233 g, 0.1879 mmol) in acetone with a small amount of MeOH. The solution was stirred magnetically for approximately 40 minutes while the color changed from orange to clear yellow. The solvent was removed under reduced pressure and the residue dissolved in minimal DCM and filtered. Addition of hexanes gave a yellow powder (0.0554 g, 73%). Single crystals were grown from vapor diffusion of hexanes into DCM (Figure 4). **^{1}H NMR** (400 MHz, $CDCl_3$, δ): 5.59 (s, 1H, C(O)C*H*C(O)), 2.05 (s, 3H, C(O)CH_3), 1.59 (s, 15H, Cp*Me). **^{13}C NMR** (101 MHz, $CDCl_3$, δ): 192.3 (*C*(O)CH_3), 165.9 (unresolved q, J=33.1 Hz, *C*(O)CF_3), 118.3 (unresolved q, J=283.8 Hz, C(O)*C*F_3), 96.2 (C(O)*C*HC(O)), 84.3 (Cp**C*), 29.5 (C(O)*C*H_3), 8.8 (Cp*Me). **^{19}F NMR** (376 MHz, $CDCl_3$, δ): -74.77. **HRMS/ESI+** (*m/z*): Calc. for $C_{15}H_{19}F_3O_2[^{193}Ir]$: 481.0961; Found: 481.0970.

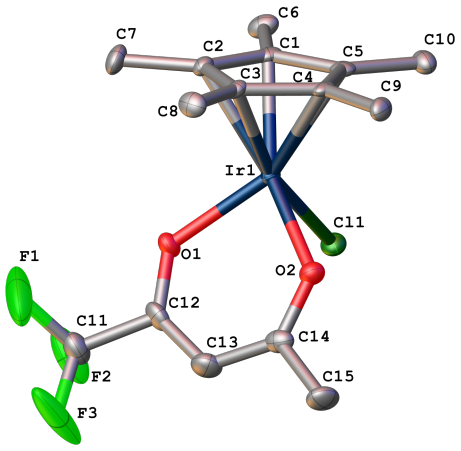

Figure 4: ADP plot of **1-Ir** (CCDC: 1902049). Hydrogen atoms omitted for clarity. Ellipsoids shown at 50% probability.

*Synthesis of **2-Ir**.* A round-bottom flask was charged with $[Cp^*IrCl_2]_2$ (0.0504 g, 0.0633 mmol) and hfacNa (0.0612 g, 0.2660 mmol) in dry DCM. The orange solution was stirred magnetically for 2 hours then filtered. The solvent was removed via reduced pressure. Addition of hexanes to the orange oily residue gave an orange powder that was collected on a frit and washed with cold hexanes, giving **2-Ir** as the exclusive product via NMR (0.0456 g, 64%). Single crystals of **2-Ir** (Figure 5), **3-Ir**, and **4-Ir** grew from vapor diffusion of hexanes into DCM. Analysis for **2-Ir**: **^{1}H NMR** (400 MHz, $CDCl_3$, δ): 5.93 (s, 1H, C(O)C*H*C(O)), 1.61 (s, 15H, Cp*Me). **^{13}C NMR** (101 MHz, $CDCl_3$, δ): 172.4 (q, J=35.3 Hz, *C*(O)CF_3), 117.6 (q, J=284.6 Hz, (C(O)*C*F_3)), 92.0–91.8 (m, C(O)*C*HC(O)), 85.5 (Cp**C*), 8.8 (Cp*Me). **^{19}F NMR** (376 MHz, $CDCl_3$, δ): -75.49.

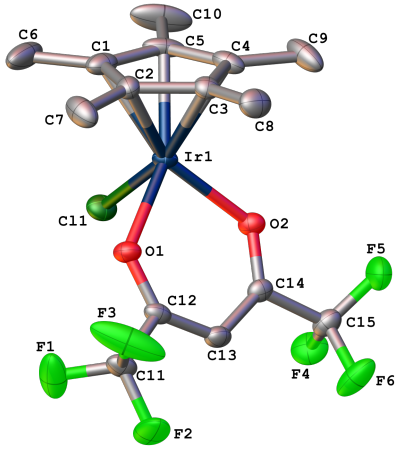

Figure 5: ADP plot of **2-Ir** (CCDC: 1996243). Hydrogen atoms omitted for clarity. Ellipsoids shown at 50% probability.

*Synthesis of **3-Ir**.* AgTFA (0.0080 g, 0.0361 mmol) was added to a sample of **2-Ir** in $CDCl_3$ (0.0206 g, 0.0361 mmol). The solution was heated at 40 °C for 2 hours while the color changed from orange to gold. The solution was then filtered and analyzed to show quantitative conversion to **3-Ir** (0.0234

g, 100%). Single crystals of **3-Ir** (Figure 6) were grown from vapor diffusion of hexanes into DCM. **^{1}H NMR** (400 MHz, $CDCl_3$, δ): 5.96 (s, 1H, C(O)C*H*C(O)), 1.62 (s, 15H, Cp*Me). **^{13}C NMR** (101 MHz, $CDCl_3$, δ): 173.1 (q, J=35.6 Hz, hfac *C*(O)CF_3), 161.6 (q, J=36.6 Hz, TFA O*C*(O)CF_3), 117.7 (q, J=284.3 Hz, hfac C(O)*C*F_3), 116.2 (q, J=290.5 Hz, TFA OC(O)*C*F_3), 91.4–91.2 (m, C(O)*C*HC(O)), 85.2 (Cp**C*), 9.2 (Cp*Me). **^{19}F NMR** (376 MHz, $CDCl_3$, δ): -74.74 (s, 3F), -75.57 (s, 6F).

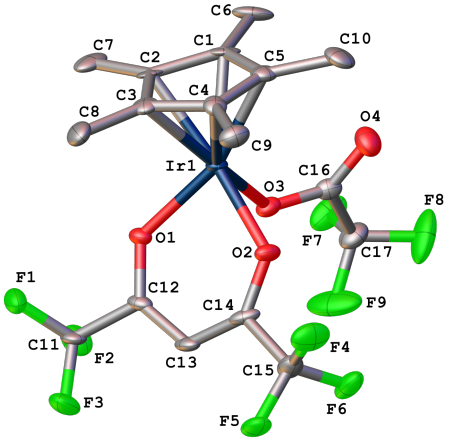

Figure 6: ADP plot of **3-Ir** (CCDC: 1902050). Hydrogen atoms omitted for clarity. Ellipsoids shown at 50% probability.

*Synthesis of **4-Ir**.* AgTFA (0.0214 g, 0.0969 mmol) and 4 Å mol sieves were stirred in benzene at room temperature for approximately one hour before $[Cp^*IrCl_2]_2$ (0.0300 g, 0.0377 mmol) was added, which resulted in a color change to yellow with pale colored precipitate. The solution was stirred magnetically for 1 hour, then syringe filtered. The solvent was removed under reduced pressure to give a yellow microcrystalline product (0.0282 g, 79%). Crystals of **4-Ir** (Figure 7) grew from vapor diffusion of hexanes into DCM. **^{1}H NMR** (400 MHz, $CDCl_3$, δ): 1.51 (s, 15H, Cp*Me). **^{13}C NMR** (101 MHz, $CDCl_3$, δ): 115.9 (unresolved q, J=290.9 Hz, (C(O)*C*F_3)), 85.8 (Cp**C*), 9.2 (Cp*Me). **^{19}F NMR** (376 MHz, $CDCl_3$, δ): -73.50.

*Synthesis of **5-Ir**.* $Na_2CO_3 \cdot H_2O$ (0.0197 g, 0.1589 mmol) was added to a solution of **2-Ir** (0.0447 g, 0.0784 mmol) in MeOH (10 mL), affecting an immediate color change from orange to yellow. The solution was stirred at room temperature for 30 minutes. The solvent was removed under reduced pressure, DCM was added, and the solution was filtered. Addition of hexanes gave a yellow powder that was collected on a frit and washed with cold hexanes (0.0328 g, 73%). Single crystals of **5-Ir** (Figure 8) grew from vapor diffusion of hexanes into acetone. PXRD of the bulk powder was found to match the powder pattern calculated from the single crystal of **5-Ir**. **^{1}H NMR** (400 MHz, $CDCl_3$, δ): 5.80 (s, 2H, C(O)C*H*C(O))), 3.37 (s, 3H, O*H*) 1.57 (s, 15H, Cp*Me). **^{13}C NMR** (101 MHz, $CDCl_3$, δ): 86.7–86.4 (m, C(O)*C*HC(O)), 81.0 (Cp**C*), 9.2 (Cp*Me). **^{19}F NMR** (376 MHz, $CDCl_3$, δ):

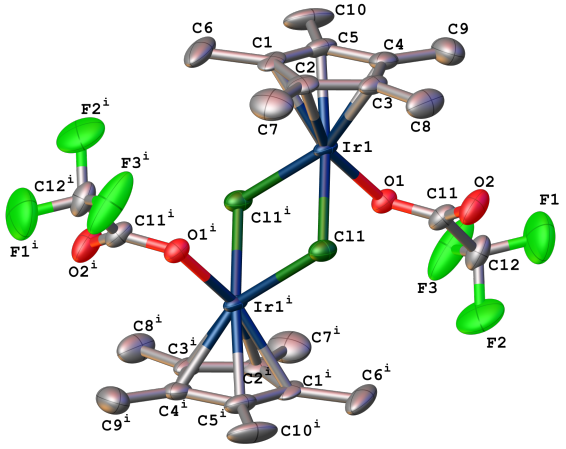

Figure 7: ADP plot of **4-Ir** (CCDC: 1902053). Atoms generated by inversion are denoted with a superscript i following the label. Hydrogen atoms omitted for clarity. Ellipsoids shown at 50% probability.

-76.79.

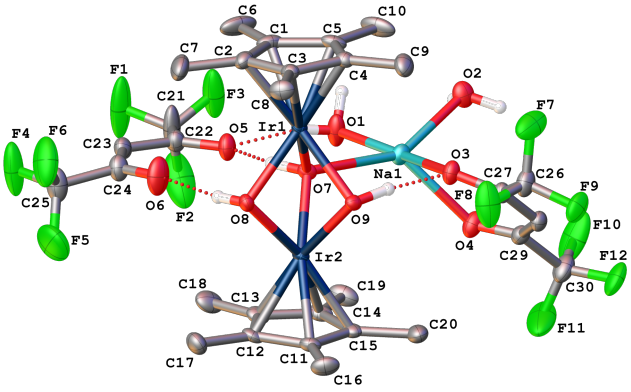

Figure 8: ADP plot of **5-Ir** (CCDC: 1996249). Hydrogen atoms on the Cp* and hfac moieties are omitted for clarity. Ellipsoids shown at 50% probability.

*Synthesis of **6-Ir** and **7-Ir**.* $Na_2CO_3 \cdot H_2O$ (0.0049 g, 0.0398 mmol) was added to a solution of **3-Ir** (0.0234 g, 0.0361 mmol) in MeOH (3 mL). The solution was stirred at room temperature for 30 minutes. The solvent was removed under reduced pressure, $CDCl_3$ was added, and the solution was filtered. and analyzed via NMR to reveal multiple signals. Single crystals of **5-Ir** and **6-Ir** (Figures 8 and 9, respectively) were grown from vapor diffusion of EtOEt into a solution of MeOH and DCM. No yield can be given for this reaction, as the crystalline components are most likely degradation products. A third unique type of crystal was found in the same sample; however, the quality of these crystals was too low for X-ray diffraction. Over time, a large number of crystals of **7-Ir** (Figure 10) also grew from this solution. These crystals were able to be isolated and characterized via NMR. NMR analysis is given for **7-Ir**. **^{1}H NMR** (400 MHz, $CDCl_3$, δ):

3.60 (s, 3H, O*H*), 1.60 (s, 30H, Cp*Me). **^{13}C NMR** (101 MHz, $CDCl_3$, δ): 80.4 (Cp**C*), 9.5 (Cp*Me). **^{19}F NMR** (376 MHz, $CDCl_3$, δ): -75.80.

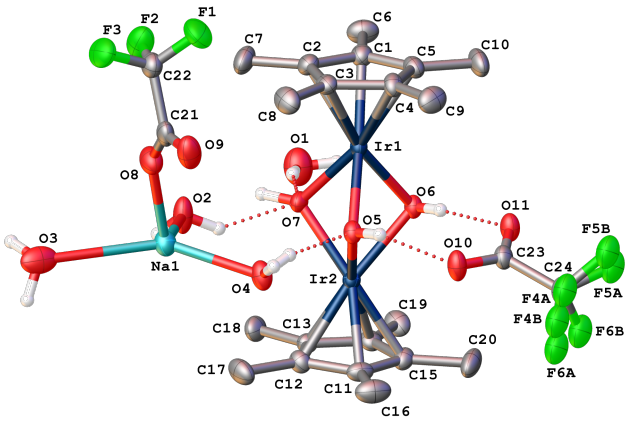

Figure 9: ADP plot of **6-Ir** (CCDC: 1996248). Hydrogen atoms on the Cp* moiety are omitted for clarity. Ellipsoids shown at 50% probability.

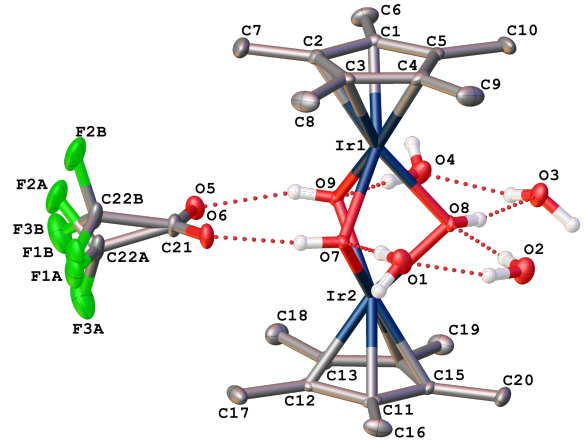

Figure 10: ADP plot of **7-Ir** (CCDC: 1902054). Hydrogen atoms on the Cp* moiety are omitted for clarity. Ellipsoids shown at 50% probability.

*Synthesis of **8-Ir**.* A round-bottom flask was charged with $[Cp^*IrCl_2]_2$ (0.0325 g, 0.0408 mmol) and hfacNa (0.0219 g, 0.0952 mmol) in DCM (10 mL). The solution was stirred magnetically for 48 hours, then MeOH (2 mL) and $Na_2CO_3 \cdot H_2O$ (0.0134 g, 0.1081 mmol) were added, affecting a color change from orange to clear yellow. After stirring overnight, the solution was diluted with DCM (15 mL), washed with water (2x10 mL), and brine (10 mL). The yellow organic layer was dried over Na_2SO_4 and the solvent was removed via reduced pressure, yielding a yellow powdery residue (0.0288 g, 77%). Identical single crystals of **8-Ir** (Figure 11) grew from $CDCl_3$ and from D_2O. Over time, single crystals of **6-Ir** and **7-Ir** also grew from the same solution. Analysis for **8-Ir**: **^{1}H NMR** (400 MHz, $CDCl_3$, δ): 5.70 (s, 1H, C(O)C*H*C(O))), 3.53 (s, 3H, O*H*) 1.58 (s, 15H, Cp*Me). **^{13}C NMR** (101 MHz, $CDCl_3$, δ): 86.5–85.9 (m, C(O)*C*HC(O)), 80.8 (Cp**C*), 9.0 (Cp*Me). **^{19}F NMR** (376 MHz, $CDCl_3$, δ): -76.70.

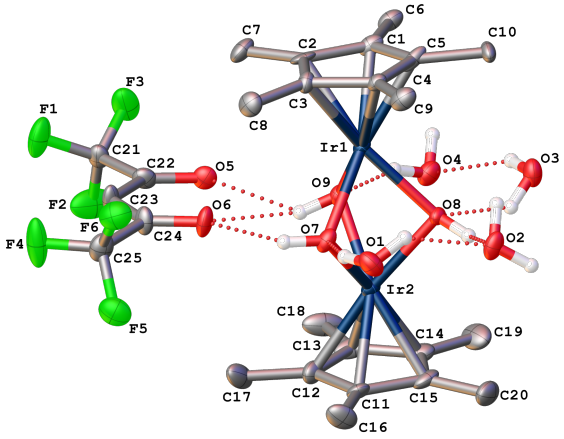

Figure 11: ADP plot of **8-Ir** (CCDC: 1996245). Hydrogen atoms on the Cp* and hfac moieties are omitted for clarity. Ellipsoids shown at 50% probability.

*Synthesis of **9-Ir**.* A round-bottom flask was charged with $[Cp^*IrCl_2]_2$ (0.0509 g, 0.0639 mmol) and NaTFA (0.0265 g, 0.1948 mmol) in a 1:1:1 mixture of acetone, MeOH, and DCM (12 mL). The solution was stirred magnetically for 60 minutes while the color changed from orange to yellow with pale colored precipitate. The solution was washed with saturated aqueous Na_2CO_3 (10 mL) and brine, then dried over Na_2SO_4. Addition of hexanes gave a pale yellow powder (0.0170 g) that was collected on a frit and washed with hexanes. Single crystals of **7-Ir** grew from vapor diffusion of hexanes into an acetone solution of the bulk powder. Single crystals of **9-Ir** (Figure 12) grew from slow evaporation of a $CDCl_3$ solution of the bulk powder. No yield can be given for **9-Ir**, which is most likely a degradation product. Analysis for **9-Ir**: **^{1}H NMR** (400 MHz, $CDCl_3$, δ): 1.68 (s, 15H, Cp*Me). **^{13}C NMR** (101 MHz, $CDCl_3$, δ): 80.8 (Cp**C*), 9.7 (Cp*Me).

*Synthesis of **10-Ir**.* A round-bottom flask was charged with $[Cp^*IrCl_2]_2$ (0.0500 g, 0.0628 mmol) and hfacNa (0.0332 g, 0.1443 mmol) in acetone (10 mL) with MeOH (3 mL). The solution was stirred magnetically for approximately 60 minutes while the color changed from orange to clear yellow. The solvent was removed via reduced pressure and the residue was dissolved in DCM and filtered. Addition of hexanes gave a pale yellow powder that was collected on a frit and washed with cold hexanes (0.0402 g). NMR analysis in $CDCl_3$ and d-acetone shows a mixture of products. Single crystals of **2-Ir**, **3-Ir**, **5-Ir**, **7-Ir**, and **10-Ir** (Figure 13) were grown from vapor diffusion of hexanes into DCM or acetone. No yield can be given for **10-Ir**, as it is most likely a degradation product.

*Synthesis of **11-Ir**.* A round-bottom flask was charged with $[Cp^*IrCl_2]_2$ (0.0600 g, 0.0753 mmol) and $Na_2CO_3 \cdot H_2O$ (0.0196 g, 0.1582 mmol) in acetone (10 mL). Hexafluoroacetylacetone (0.0219 mL, 0.1544 mmol) was added drop-

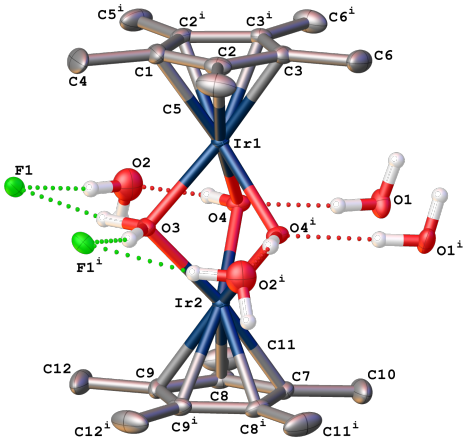

Figure 12: ADP plot of **9-Ir** (CCDC: 1996250) Atoms related by a mirror plane are denoted with a superscript i following the label. Hydrogen atoms on the Cp* moiety are omitted for clarity. Ellipsoids shown at 50% probability.

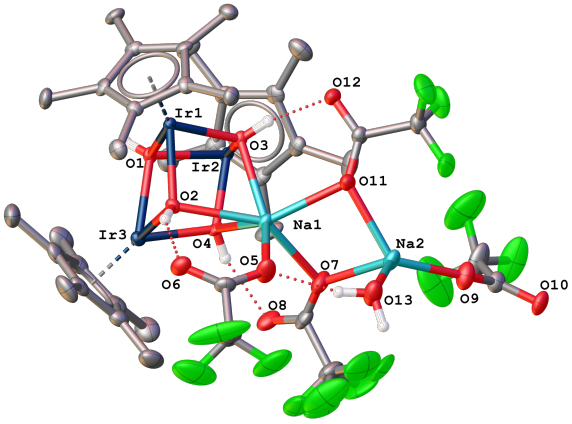

Figure 13: ADP plot of **10-Ir** (CCDC: 1902052). Hydrogen atoms on the Cp* moieties and non-coordinating solvent (acetone) are omitted for clarity. Labels are shown only for Ir, Na, and O atoms. Ellipsoids shown at 50% probability.

wise to the stirring mixture. After 25 min, MeOH (2 mL) was added. The solution was stirred magnetically for approximately 60 minutes while the color changed from orange to clear yellow. The solvent was removed via reduced pressure and the residue was dissolved in DCM and filtered. Addition of hexanes gave a yellow-brown powder (0.0671 g) that was collected on a frit and washed with cold hexanes. NMR analysis in $CDCl_3$ and d-acetone shows a mixture of products. Crystals of **7-Ir** and **11-Ir** (Figure 14) grew from vapor diffusion of hexanes into a solution of acetone and DCM. No yield can be given for **11-Ir**, as it is most likely a degradation product.

6.3.2. Rhodium complexes

Synthesis of ***1-Rh***. A round-bottom flask was charged with $[Cp^*RhCl_2]_2$ (0.0508 g, 0.0822 mmol), trifluoroacetylacetone (0.0219 mL, 0.1808 mmol), and $Na_2CO_3 \cdot H_2O$ (0.0273 g, 0.2202 mmol) in acetone with a small amount of MeOH.

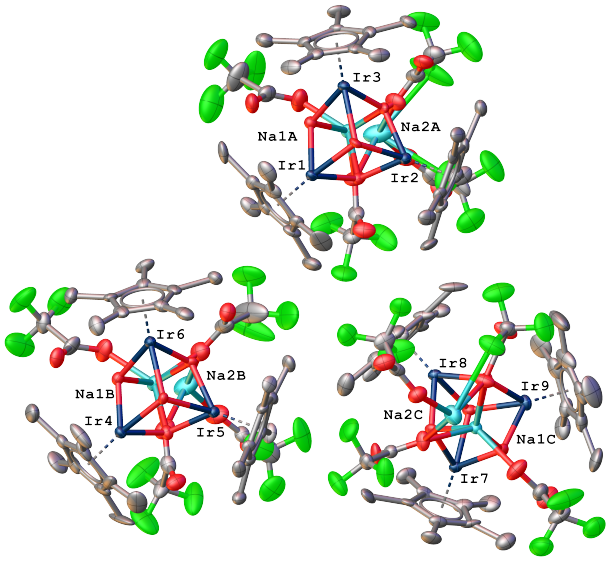

Figure 14: ADP plot of **11-Ir** (CCDC: 1996247). Hydrogen atoms omitted for clarity. Labels are shown only for Ir and Na atoms. Ellipsoids shown at 50% probability.

The solution was stirred magnetically for approximately 40 minutes while the color changed from red to clear orange. The solvent was removed under reduced pressure and the residue dissolved in minimal DCM and filtered. Addition of hexanes gave an orange microcrystalline powder (0.0622 g, 89%). Single crystals of **1-Rh** (Figure 15) were grown from vapor diffusion of hexanes into DCM. **^{1}H NMR** (400 MHz, $CDCl_3$, δ): 5.49 (s, 1H, C(O)C*H*C(O)), 2.13 (s, 3H, C(O)CH_3), 1.63 (s, 15H, Cp*Me). **^{13}C NMR** (101 MHz, $CDCl_3$, δ): 194.5 (*C*(O)CH_3), 168.0 (unresolved q, J=32.4 Hz,*C*(O)CF_3), 118.3 (unresolved q, J=284.8 Hz, C(O)*C*F_3), 94.2 (m, C(O)*C*HC(O)), 92.9 (d, J_{FH}=9.2 Hz, Cp**C*), 29.7 (s, C(O)*C*H_3), 8.6 (Cp*Me). **^{19}F NMR** (376 MHz, $CDCl_3$, δ): -74.67. **HRMS/ESI+** (*m/z*): Calc. for $C_{15}H_{19}O_2F_3Rh$: 391.0387; Found: 391.0398.

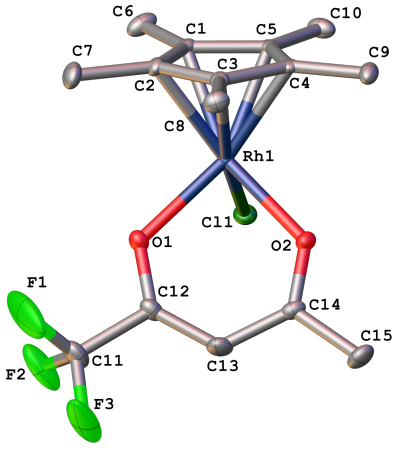

Figure 15: ADP plot of **1-Rh** (CCDC: 1902051). Hydrogen atoms are omitted for clarity. Ellipsoids shown at 50% probability.

*Synthesis of **2-Rh** and **12-Rh**.* In the glovebox, a Schlenk flask was charged with sodium hexafluoroacetylacetonate (0.0270 g, 0.1174 mmol). The flask was brought out of the glovebox, and $[Cp^*RhCl_2]_2$ (0.0299 g, 0.0484 mmol) and nitrogen-purged DCM (10 mL) were quickly added. The solution was stirred magnetically for approximately 2 hours, then filtered under air. The solvent was removed under reduced pressure and the orange residue dissolved in minimal DCM. Addition of hexanes gave an orange microcrystalline powder (0.0325 g, 70%). Single crystals of **2-Rh** (Figure 16), **4-Rh**, and **12-Rh** (Figure 17) grew from vapor diffusion of hexanes into DCM or acetone. No yield can be given for **12-Rh**, as it is most likely a degradation product. Analysis for **2-Rh**: **^{1}H NMR** (400 MHz, $CDCl_3$, δ): 5.85 (s, 1H, C(O)C*H*C(O)), 1.66 (s, 15H, Cp*Me). **^{13}C NMR** (101 MHz, $CDCl_3$, δ): 175.3 (unresolved q, J=34.8 Hz,*C*(O)CF_3), 117.4 (unresolved q, J=287.8 Hz, C(O)*C*F_3), 93.8 (d, J=9.7 Hz, Cp**C*), 89.3 (m, C(O)*C*HC(O)), 8.7 (Cp*Me). **^{19}F NMR** (376 MHz, $CDCl_3$, δ): -75.51. **HRMS/ESI+** (*m/z*): Calc. for $C_{15}H_{16}F_6O_2Rh^+$: 445.0104; Found: 445.0105.

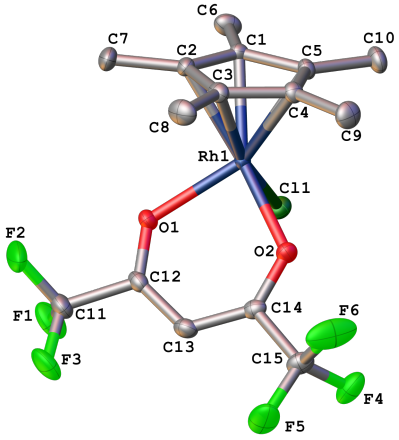

Figure 16: ADP plot of **2-Rh** (CCDC: 1996246) Hydrogen atoms omitted for clarity. Ellipsoids shown at 50% probability.

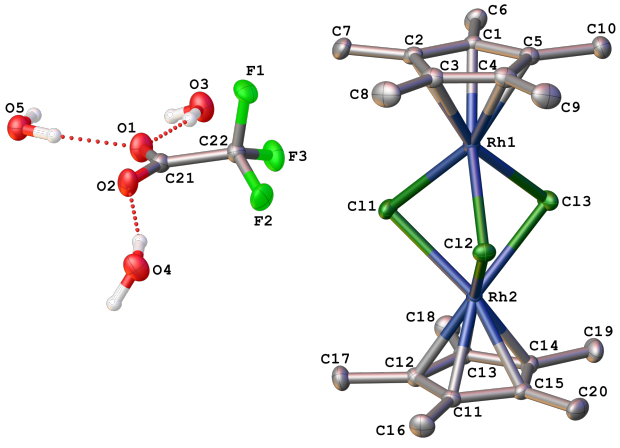

Figure 17: ADP plot of **12-Rh** (CCDC: 1996251) Hydrogen atoms omitted for clarity. Ellipsoids shown at 50% probability.

*Synthesis of **4-Rh**.* AgTFA (0.0244 g, 0.1105 mmol) and 4 Å mol sieves were stirred in benzene at room temperature for approximately one hour before $[Cp^*RhCl_2]_2$ (0.0299 g, 0.0484 mmol) was added, which resulted in a color change to orange with pale colored precipitate. The solution was stirred magnetically for 1 hour, then syringe filtered. The solvent was removed under reduced pressure to give an orange microcrystalline product (0.0160 g, 43%). Single crystals of **4-Rh** (Figure 18) grew from vapor diffusion of hexanes into DCM. **^{1}H NMR** (400 MHz, $CDCl_3$, δ): 1.54 (s, 15H, Cp*Me). **^{13}C NMR** (101 MHz, $CDCl_3$, δ): 94.1 (d, J=9.2 Hz, Cp**C*), 9.1 (Cp*Me). **^{19}F NMR** (376 MHz, $CDCl_3$, δ): -73.69.

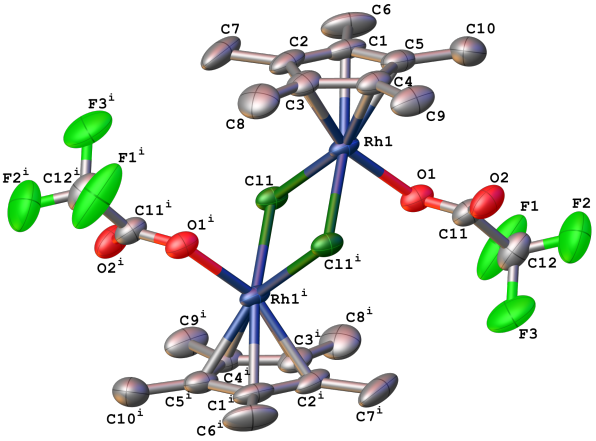

Figure 18: ADP plot of **4-Rh** (CCDC: 1996244). Atoms generated by inversion are denoted with a superscript i following the label. Hydrogen atoms omitted for clarity. Ellipsoids shown at 50% probability.

Declaration of competing interest

The authors declare that they have no known competing financial interests or personal relationships that could have appeared to influence the work reported in this paper.

Acknowledgments

The authors thank Dr. Carla Slebodnick, Loren Brown, and Chad Bernier for their assistance with several crystal structures. Funding for the Rigaku Oxford Diffraction Synergy diffractometer used in a portion of this study was obtained from the National Science Foundation (grant No. 1726077). We also thank the Virginia Tech Department of Chemistry for funds and supplies.

A. Supplementary Information

Comparison of experimental powder patterns with data calculated from single crystal X-ray structures, relevant bond lengths, and structure factors for all compounds characterized by XRD are included.

References

[1] P. Muraoka, D. Byun, J. I. Zink, Excited states and gas phase photofragmentation of palladium and platinum hexafluoroacetylacetonates, Coord. Chem. Rev. 208 (2000) 193–211. doi:10.1016/S0010-8545(00)00356-8.

[2] A. W. Maverick, F. R. Fronczek, E. F. Maverick, D. R. Billodeaux, Z. T. Cygan, R. A. Isovitsch, Structures of Anhydrous and Hydrated Copper(II) Hexafluoroacetylacetonate, Inorg. Chem. 41 (2002) 6488–6492. doi:10.1021/ic020448w.

[3] G. G. Condorelli, G. Malandrino, I. L. Fragalà, Engineering of molecular architectures of β-diketonate precursors toward new advanced materials, Coord. Chem. Rev. 251 (2007) 1931–1950. doi:10.1016/j.ccr.2007.04.016.

[4] V. Y. Vasilyev, N. B. Morozova, T. V. Basova, I. K. Igumenov, A. Hassan, Chemical vapour deposition of Ir-based coatings: chemistry, processes and applications, RSC Adv. 5 (2015) 32034–32063. doi:10.1039/C5RA03566J.

[5] J. P. Collman, R. L. Marshall, W. L. Young, S. D. Goldby, Reactions of Metal Chelates. III. Nitration and Formylation of Metal Acetylacetonates, Inorg. Chem. 1 (1962) 704–710. doi:10.1021/ic50003a052.

[6] L. Davignon, J. Manoli, A. Dereigne, Étude cristallographique des hexafluoroacétylacétonates de rhodium(III) et d'iridium(III), J. Less Common Met. 21 (1970) 341–344. doi:10.1016/0022-5088(70)90156-6.

[7] Q. Zhang, X. Yan, H. Zhang, J. Zhang, Preparation of tris(hexafluoroacetylacetonato)iridium., 2006.

[8] S. C. Chattoraj, R. E. Sievers, New rhodium chelates of hexafluoroacetylacetone., Inorg. Chem. 6 (1967) 408–411. doi:10.1021/ic50048a054.

[9] S. Cenini, R. Ugo, F. Bonati, The preparation and properties of some mixed binuclear rhodium(II) acetato-β diketonato compounds, Inorganica Chim. Acta 1 (1967) 443–447. doi:10.1016/S0020-1693(00)93220-1.

[10] J. H. Potgieter, J. G. Leipoldt, S. S. Basson, An improved synthesis of [Rh(β-diketone(COD)] complexes, South African J. Chem. 12 (1988) 120–121.

[11] Y. Kitamura, J. Leipoldt, A. Roodt, Spectrophotometric study of the methoxide addition to hexafluoroacetylacetonato complexes of Co(III) and the crystal structure of β-[Co(trien)(hfacOCH3)](ClO4), Inorganica Chim. Acta 149 (1988) 125–129. doi:10.1016/S0020-1693(00)90578-4.

[12] T. Katou, Y. Yamamoto, K. Kuroda, K. Watanabe, Y. Kitamura, Preparation and pH dependent reversible color change of (hexafluoroacetylacetonato)bis(ethylenediamine)chromium(III) complex, Inorganica Chim. Acta 180 (1991) 13–14. doi:10.1016/S0020-1693(00)83058-3.

[13] E. Bouwman, J. C. Huffman, E. B. Lobkovsky, G. Christou, H. L. Tsai, D. N. Hendrickson, A new fluorinated tetraalkoxide ligand derived from the hydration of hexafluoroacetylacetone, Inorg. Chem. 31 (1992) 4436–4438. doi:10.1021/ic00048a002.

[14] C. M. DuChane, L. C. Brown, V. S. Dozier, J. S. Merola, Synthesis, Characterization, and Antimicrobial Activity of Rh III and Ir III β-Diketonato Piano-Stool Compounds, Organometallics 37 (2018) 530–538. doi:10.1021/acs.organomet.7b00742.

[15] C. R. Groom, I. J. Bruno, M. P. Lightfoot, S. C. Ward, The Cambridge Structural Database, Acta Crystallogr. Sect. B Struct. Sci. Cryst. Eng. Mater. 72 (2016) 171–179. doi:10.1107/S2052520616003954.

[16] A. Nutton, P. M. Bailey, P. M. Maitlis, Pentamethylcyclopentadienylrhodium and -iridium complexes. Part 29. Syntheses and X-ray structure determinations of [{Rh(C5Me5)}2(OH)3]OH·11H2O and [{Ir(C5Me5)}2(OH)3]O2CMe·14H2O and related complexes, J. Chem. Soc., Dalton Trans. (1981) 1997–2002. doi:10.1039/DT9810001997.

[17] P. A. Abramov, C. Vicent, N. B. Kompankov, A. L. Gushchin, M. N. Sokolov, Coordination of {C5Me5Ir}2+to [M6O19]8-(M = Nb, Ta) - Analogies and Differences between Rh and Ir, Nb and Ta, Eur. J. Inorg. Chem. 2016 (2016) 154–160. doi:10.1002/ejic.201501051.

[18] L. Dadci, H. Elias, U. Frey, A. Hörnig, U. Koelle, A. E. Merbach, H. Paulus, J. S. Schneider, π-Arene Aqua Complexes of Cobalt, Rhodium, Iridium, and Ruthenium: Preparation, Structure, and Kinetics of Water Exchange and Water Substitution, Inorg. Chem. 34 (1995) 306–315. doi:10.1021/ic00105a048.

[19] J. T. Park, T. Nishioka, T. Suzuki, K. Isobe, Synthesis and Crystal Structure of [(IrCp*)2(μ-OH)3]2(Cr2O7)·8H2O (Cp* = η5-C5Me5). A Novel Two-Dimensional Hydrogen-Bonding Network, Bull. Chem. Soc. Jpn. 67 (1994) 1968–1971. doi:10.1246/bcsj.67.1968.

[20] C. F. Macrae, P. R. Edgington, P. McCabe, E. Pidcock, G. P. Shields, R. Taylor, M. Towler, J. Van De Streek, Mercury: Visualization and analysis of crystal structures, J. Appl. Crystallogr. 39 (2006) 453–457. doi:10.1107/S002188980600731X.

[21] C. F. Macrae, I. J. Bruno, J. A. Chisholm, P. R. Edgington, P. McCabe, E. Pidcock, L. Rodriguez-Monge, R. Taylor, J. Van De Streek, P. A. Wood, Mercury CSD 2.0 - New features for the visualization and investigation of crystal structures, J. Appl. Crystallogr. 41 (2008) 466–470. doi:10.1107/S0021889807067908.

[22] M. Hidai, S. Kuwata, Y. Mizobe, Synthesis and Reactivities of Cubane-Type Sulfido Clusters Containing Noble Metals, Acc. Chem. Res. 33 (2000) 46–52. doi:10.1021/ar990016y.

[23] S. A. Bartlett, E. V. Sackville, E. K. Gibson, V. Celorrio, P. P. Wells, M. Nachtegaal, S. W. Sheehan, U. Hintermair, Evidence for tetranuclear bis-μ-oxo cubane species in molecular iridium-based water oxidation catalysts from XAS analysis, Chem. Commun. 55 (2019) 7832–7835. doi:10.1039/C9CC02088H.

[24] K. Umakoshi, K. Murata, S. Yamashita, K. Isobe, Reactivity of [Cp*RhPtCl6] (Cp* = η5-C5Me5). Synthesis and structures of [(Cp*Rh)2(μ-Cl)3][PtCl5(CH3CONH2)] and [(Cp*Rh)2(μ-Cl)3]2[PtCl6], Inorganica Chim. Acta 190 (1991) 185–191. doi:10.1016/S0020-1693(00)80252-2.

[25] M. N. Vargaftik, Y. T. Struchkov, A. I. Yanovsky, P. M. Maitlis, Synthesis and X-Ray Structure of Cp*Rh(III)-Molybdate Complexes Derived from Bis(triphenylphosphineiminium) Mono- and Polymolybdates, Mendeleev Commun. 3 (1993) 247–249. doi:10.1070/MC1993v003n06ABEH000314.

[26] I. Ara, J. R. Berenguer, E. Eguizábal, J. Forniés, E. Lalinde, A. Martín, Synthesis of Novel Heterotetrametallic (d6-d10-d8) Polyalkynyl Complexes Starting from Heterobimetallic Chloride-Bridged (d6-d8) Compounds, Eur. J. Inorg. Chem. 2001 (2001) 1631–1640. doi:10.1002/1099-0682(200106)2001:6<1631::AID-EJIC1631>3.0.CO;2-6.

[27] W. S. Han, S. W. Lee, Rhodium(III)-mediated cycloaddition of alkynes: reactivity of [Cp*Rh(η2-NO3)(OTf)] bearing two labile ligands, J. Organomet. Chem. 678 (2003) 102–107. doi:10.1016/S0022-328X(03)00451-0.

[28] S. Gauthier, L. Quebatte, R. Scopelliti, K. Severin, Syntheses and structures of homo- and heterobimetallic, chloro-bridged complexes containing the RuCl 3 (AsPh3) n fragment (n=1, 2), Inorg. Chem. Commun. 7 (2004) 708–712. doi:10.1016/j.inoche.2004.03.022.

[29] L. Liu, Q.-F. Zhang, W.-H. Leung, Tri-μ-chloro-bis[(η5-pentamethylcyclopentadienyl)rhodium(III)] tetrafluoroborate, Acta Crystallogr. Sect. E Struct. Reports Online 60 (2004) m509–m510. doi:10.1107/S1600536804007226.

[30] L. S. Alekseev, F. M. Dolgushin, I. T. Chizhevsky, An efficient synthesis of 12-vertex closo-rhodacarboranes [3-(η5-C5Me5)-1-R1-2-R2-3,1,2-closo-RhC2B9H9] (R1, R2=H, Alk) via two-step reactions of [K][7-R1-8-R2-7,8-nido-C2B9H10] mono-anions with [Rh2(η5-C5Me5)2Cl4]: structural characterization of the firs, J. Organomet. Chem. 693 (2008) 3331–3336. doi:10.1016/j.jorganchem.2008.06.018.

[31] K. Q. Vuong, C. M. Wong, M. Bhadbhade, B. A. Messerle, Bi- and tri-metallic Rh and Ir complexes containing click derived bis- and tris-(pyrazolyl-1,2,3-triazolyl) N-N' donor ligands and their application as catalysts for the dihydroalkoxylation of alkynes, Dalt. Trans. 43 (2014) 7540–7553. doi:10.1039/C3DT53295J.

[32] L. Ezzedinloo, S. Shrestha, M. Bhadbhade, S. Colbran, Tri-μ-chlorido-bis[(η 5 -pentamethylcyclopentadienyl)rhodium(III)] hexafluoridophosphate from synchrotron radiation, Acta Crystallogr. Sect. E Struct. Reports Online 70 (2014) m14–m15. doi:10.1107/S1600536813032480.

[33] P. Abramov, M. Sokolov, I. Mirzaeva, A. Virovets, Coordination of SnCl3- ligands to {Cp*M}2+ (M = Rh, Ir), J. Organomet. Chem. 754 (2014) 32–38. doi:10.1016/j.jorganchem.2013.12.043.

[34] M. A. Mantell, J. W. Kampf, M. Sanford, Improved Synthesis of [CpRRhCl2]2 Complexes, Organometallics 37 (2018) 3240–3242. doi:10.1021/acs.organomet.8b00400.

[35] H. Duschner, K. Starke, Kinetics and mechanism of enolization, diol formation, and decomposition of hexafluoroacetylacetone in aqueous solution, J. Inorg. Nucl. Chem. 40 (1978) 1387–1393. doi:10.1016/0022-1902(78)80055-4.

[36] C. Reichert, J. B. Westmore, H. D. Gesser, Mass spectra of fluorinated acetylacetonate complexes, Chem. Commun. (1967) 782–783. doi:10.1039/c19670000782.

[37] S. Engmann, B. Ómarsson, M. Lacko, M. Stano, Š. Matejčík, O. Ingólfsson, Dissociative electron attachment to hexafluoroacetylacetone and its bidentate metal complexes M(hfac) 2 ; M = Cu, Pd, J. Chem. Phys. 138 (2013) 234309. doi:10.1063/1.4810877.

[38] L. S. Sharninghausen, S. B. Sinha, D. Y. Shopov, B. Choi, B. Q. Mercado, X. Roy, D. Balcells, G. W. Brudvig, R. H. Crabtree, High Oxidation State Iridium Mono-μ-oxo Dimers Related to Water Oxidation Catalysis, J. Am. Chem. Soc. 138 (2016) 15917–15926. doi:10.1021/jacs.6b07716.

[39] T. K. Michaelos, D. Y. Shopov, S. B. Sinha, L. S. Sharninghausen, K. J. Fisher, H. M. Lant, R. H. Crabtree, G. W. Brudvig, A Pyridine Alkoxide Chelate Ligand That Promotes Both Unusually High Oxidation States and Water-Oxidation Catalysis, Acc. Chem. Res. 50 (2017) 952–959. doi:10.1021/acs.accounts.6b00652.

[40] L. C. Brown, E. Ressegue, J. S. Merola, Rapid Access to Derivatized, Dimeric, Ring-Substituted Dichloro(cyclopentadienyl)rhodium(III) and Iridium(III) Complexes, Organometallics 35 (2016) 4014–4022. doi:10.1021/acs.organomet.6b00580.

[41] Agilent, CrysAlis PRO, Agilent Technologies Ltd, Yarnton, Oxfordshire, England, 2014.

[42] G. M. Sheldrick, SHELXT – Integrated space-group and crystal-structure determination, Acta Crystallogr. Sect. A Found. Adv. 71 (2015) 3–8. doi:10.1107/S2053273314026370.

[43] O. V. Dolomanov, L. J. Bourhis, R. J. Gildea, J. A. K. Howard, H. Puschmann, IUCr, OLEX2: a complete structure solution, refinement and analysis program, J. Appl. Crystallogr. 42 (2009) 339–341. doi:10.1107/S0021889808042726.

[44] I. J. Bruno, J. C. Cole, P. R. Edgington, M. Kessler, C. F. Macrae, P. McCabe, J. Pearson, R. Taylor, New software for searching the Cambridge Structural Database and visualizing crystal structures, Acta Crystallogr. Sect. B Struct. Sci. 58 (2002) 389–397. doi:10.1107/S0108768102003324.